Muon-electron lepton-flavor-violating transitions: Shell-model calculations of transitions in ^{27}Al

J. Kostensalo and J. Suhonen

University of Jyvaskyla, Department of Physics, P.O. Box 35, FI-40014, Finland

O. Civitarese

Department of Physics, University of La Plata, and IFLP-CONICET, Argentina, 49 y 115. c.c.67 (1900), La Plata. Argentina

In this paper we present the results of large-scale shell-model calculations of muon-to-electron lepton-flavor-violating transitions for the case of the target nucleus ^{27}Al. We extend the previous shell-model calculations, done in the sd model space, by including also the p orbitals in order to see whether the negative-parity states produce any significant effect in the conversion rate. The analysis of the results shows the dominance of coherent transitions mediated by isovector operators and going by the ground state of the target, with practically null influence of excited positive- or negative-parity states.

I. INTRODUCTION

The nonzero mass of the neutrino allows for a variety of lepton-flavor-violating processes, forbidden in the standard model of particle physics. One of these many processes is $\mu \to e$ conversion [1–3], in which a bound $1S$ muon is captured by the nucleus and an electron is emitted with energy $E_e \approx m_\mu$. Other lepton-flavor-violating processes include $\mu \to e\gamma$, $\mu \to e\bar{e}e$, $\tau \to \mu\gamma$, and $\tau \to e\gamma$. In minimal extensions of the standard model, in which massive neutrinos are included, the lepton-flavor-violating processes would be suppressed by the ratio of the masses of the neutrino and the weak boson, $(m_\nu/m_W)^4 \sim 10^{-48}$–$10^{-50}$, and therefore be experimentally unobservable. The observation of such a conversion would therefore point to the existence of new massive particles, as was pointed out in Ref. [4].

So far, only upper limits for the branching ratio

$$R_{\mu e^-} = \frac{\Gamma(\mu^- \to e^-)}{\Gamma(\mu^- \to \nu_\mu)} \qquad (1)$$

have been determined experimentally. The measured upper limits are at the 90% confidence level $R_{\mu e^-}(\text{Au}) < 7 \times 10^{-13}$ for gold [5], $R_{\mu e^-}(\text{Ti}) < 6.1 \times 10^{-13}$ [6] for titanium, and $R_{\mu e^-}(\text{Pb}) < 4.6 \times 10^{-11}$ for lead [7]. The Comet [8] and Mu2e [9] experiments aim at reaching single-event sensitivities $\sim 2.5 \times 10^{-17}$, corresponding to $< 6 \times 10^{-17}$ upper limit at 90% confidence level. For muon-flavor-violating processes the most restrictive limit is currently $R_{\mu \to e\gamma} < 4.2 \times 10^{-13}$ [10]. For τ-flavor-violating decays the experimental upper limits are several magnitudes higher, with $R_{\tau \to e\gamma} < 3.3 \times 10^{-8}$ and $R_{\tau \to \mu\gamma} < 4.4 \times 10^{-8}$ [11].

The nuclear matrix elements related to the $\mu^- \to e^-$ conversion have been previously studied in Ref. [12]. The nuclear-structure calculations were done using the nuclear shell model with the sd shell as the valence space. The experimentally measurable coherent channel was found to

be clearly dominant. The calculations also showed a clear vector-isoscalar dominance.

In the present paper we extend the shell-model valence space to include both the p and sd shells using a realistic effective interaction. In this way the potentially significant incoherent contributions with negative parity final states can be included. This also changes the occupation of the p-shell orbitals, which affects the important monopole part in the dominating coherent channel. The larger model space, however, increases the required computational burden significantly. For example the m-scheme dimensions for the $1/2^+$ states is 80 115 in the sd shell but 61 578 146 in the p-sd model space. Therefore, some limitations to the number of computed shell-model states are made. The coherent and incoherent contributions are calculated in order to find the ratio between the coherent and total $\mu^- \to e^-$ conversion rates. This ratio is needed, since experimentally only the coherent channel is measurable due to the lack of background events such as muon decay in orbit and radiative muon capture followed by e^+e^- pair creation [13].

Since the formalism [14–20] is rather well known we shall restrict the presentation of it in Sec. II to the minimum needed to allow for a comprehensible reading of the paper. In the following sections we will introduce the definitions of the participant nuclear matrix elements as well as the basic ingredients of the shell-model procedure. The results of the calculations are presented and discussed in Sec. IV and our conclusions are drawn in Sec. V.

II. FORMALISM

Various extensions to the standard model of particle physics allows for several possible mechanisms for $\nu^- \to e^-$ conversion, such as the exchange of virtual photons, a W boson, or a neutral Z boson [1–3], conversion by Higgs-particle exchange [15,16], by supersymmetric (SUSY) particles [21], or by R-parity-violating mechanisms [22]. The operators

TABLE I. Coefficients for each of the processes contributing to the $\mu^- \to e^-$ conversion in nuclei. The expressions of these coefficients are given in Ref. [12].

Process	$C_{\text{vector}}(\text{neutrons})$	$C_{\text{vector}}(\text{protons})$	$C_{\text{axial-vector}}(\text{neutrons})$	$C_{\text{axial-vector}}(\text{protons})$
W-exchange	1.083	1.917	0.017	−1.017
SUSY Z-exchange	3.230	−0.230	4.278	−4.278
photonic	0.0	1.0	0.0	0.0

related to the hadronic vertices of the relevant Feynman diagrams, needed for the calculation of the $\mu^- \to e^-$ conversion mechanism mediated by interactions with nucleons, are of vector and axial-vector type. They can be written as

$$\mathbf{O}_{\text{vector}} = \sum_{k=p,n} C_{\text{vector}}(k)e^{-iqr_k}$$

$$\mathbf{O}_{\text{axial-vector}} = -\frac{1}{\sqrt{3}} \sum_{k=p,n} C_{\text{axial-vector}}(k)(\sigma_k)e^{-iqr_k}, \quad (2)$$

where the summations run over all nucleons and the couplings $[C_{\text{vector}}(k), C_{\text{axial-vector}}(k)]$ depend on the adopted mechanism for the $\mu^- \to e^-$ conversion [3]. Their values are given in Table I. We use the same coupling constants as in the previous shell-model study [12]. Therefore, differences between the present and previous results are purely due to the differences in the nuclear-structure calculations, and not blurred by adjustments made to the couplings.

The square of the matrix elements of the vector and axial-vector operators entering the vertices where the leptonic and nucleonic currents exchange bosons [23] are expressed in terms of the summation

$$M^2 = S_V + 3\,S_A$$

$$S_V = \frac{1}{(2J_{\text{initial}}+1)} \sum_{\text{final}} \left(\frac{q_f}{m_\mu}\right)^2 \sum_\lambda |\langle f \,||\, \mathbf{T}_{\lambda\lambda\gamma=0} \,||\, i \rangle|^2$$

$$S_A = \frac{1}{(2J_{\text{initial}}+1)} \sum_{\text{final}} \left(\frac{q_f}{m_\mu}\right)^2 \sum_{\lambda\kappa} |\langle f \,||\, \mathbf{T}_{\lambda\kappa\gamma=1} \,||\, i \rangle|^2,$$

$$(3)$$

where the initial and final states belong to the target nucleus and m_μ is the muon rest mass. The tensor operators which result from the plane-wave expansion of the factor e^{-iqr_k} are of the form [24]

$$\mathbf{T}_{\lambda\kappa\gamma,\mu}(qr) = j_\kappa(qr)[\iota^\kappa Y_\kappa(\hat{\mathbf{r}})\sigma_\gamma]_{\lambda,\mu}. \quad (4)$$

In the particle representation they are written in the form

$$\mathbf{T}_{\lambda\kappa\gamma,\mu}(qr) = \frac{1}{\sqrt{2\lambda+1}} \sum_{f,i} \langle f \,||\, \mathbf{T}_{\lambda\kappa\gamma}(qr) \,||\, i \rangle [c_f^\dagger \bar{c}_i]_{\lambda,\mu},$$

$$(5)$$

where with i and f we denote the complete set of the corresponding quantum numbers needed to define a state in the single-particle basis, that is, $i(f) = (n, l, j, m)$. In standard notation n is the number of nodes, l is the orbital angular momentum and (j, m) are the total angular momentum and its z projection, respectively, of the single-particle orbit. In the previous equations the momentum transferred from the muon to the nucleons is defined by $q_f = m_\mu - E_b - E_{\text{excitation}}$, that is, by the difference between the muon mass (105.6 MeV), the binding energy of the muon in the $1S$ orbit (0.47 MeV) and the excitation energy of each of the final states of the nucleus, which participate in the process, respectively.
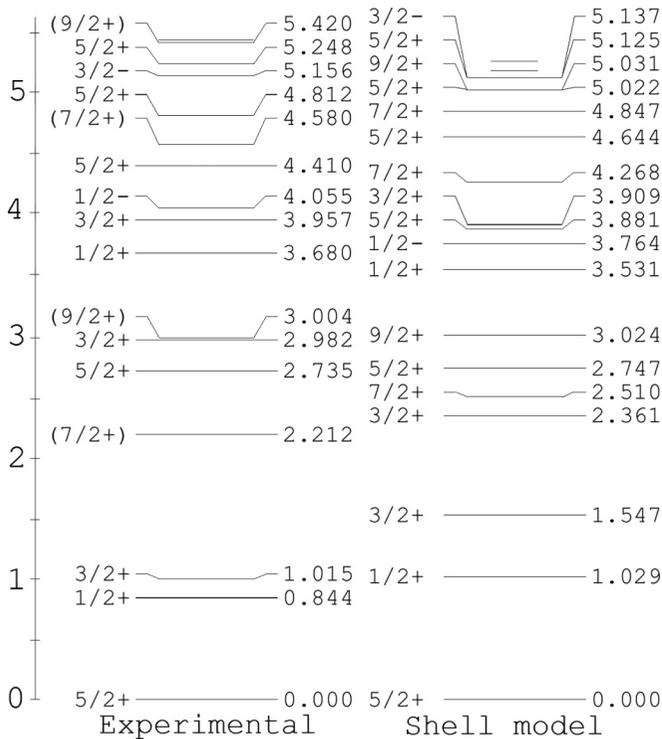
FIG. 1. Calculated (shell-model) and measured (experimental) energy levels of ^{27}Al. The experimental energy spectrum is taken from Ref. [29]. The energies are given in units of MeV.

TABLE II. Single-particle occupation factors V_j^2 for active orbitals, both for protons and neutrons.

Orbital	V_j^2 (Protons)	V_j^2 (Neutrons)
$1p_{3/2}$	3.983	3.983
$1p_{1/2}$	1.971	1.973
$2d_{5/2}$	4.237	4.9629
$2d_{3/2}$	0.468	0.596
$2s_{1/2}$	0.341	0.4837

TABLE III. Ground-state values of the calculated and experimentally extracted matrix elements for $q/(\hbar c) = 0.534$.

Quantity	Experimental value	Shell model (Ref. [12])	Shell model (present)
F_N	0.640		0.662
S_N			9.264
F_Z	0.638	0.677	0.667
S_Z			8.678
M_{coherent}^2	68.80	77.40	75.31

The ratio of the experimentally measurable coherent channel and the total conversion rate is

$$\eta = \frac{\Gamma_{\text{coh}}(\mu \to e^-)}{\Gamma_{\text{tot}}(\mu \to e^-)} \approx \frac{M_{\text{coh}}^2}{M_{\text{tot}}^2}, \qquad (6)$$

where M_{coh} is the matrix element for the coherent transition and M_{tot} is the matrix element for the total conversion rate.

III. SHELL-MODEL BASIS AND INTERACTIONS

The wave functions and one-body transition densities needed for transitions between states in ^{27}Al were computed assuming a ^{4}He core and using the $0p$, $0d$, and $1s$ orbitals as the valence space for both protons and neutrons. The Hamiltonian adopted to perform the calculations, labeled *psdmod*, was taken from Ref. [25]. It is a modified version of the interaction presented by Utsuno and Chiba in Ref. [26], which itself is a modification of the interaction PSDWBT of Warburton and Brown [27]. In the parametrization given by the *psdmod* Hamiltonian, the p-sd shell gap has been increased by 1 MeV from the original interaction of Utsuno and Chiba. The calculations were performed using the shell-model code NUSHELLX@MSU [28] on a computer cluster using four 12-core Intel Xeon E5-2680 v3 @ 2.50 GHz CPUs and took approximately 48 h. For each spin and parity ten states were calculated.

Including excitations over the p-sd shell gap allows the description of the negative parity states, which can not be described using only the sd shell. Therefore, the potentially significant spin-dipole contributions are included in the present study.

IV. RESULTS

The calculated spectrum of ^{27}Al, with displayed states up to 6 MeV, is shown in Fig. 1, where the theoretical results are compared with the available experimental data. As seen from the figure, the energy gap between the $5/2^+$ ground state and the lowest excited states, which is of the order of 1 MeV is reasonably well reproduced, although the splitting between the first $3/2^+$ state and the first $1/2^+$ state is larger in the calculations than in the data. For the rest of the spectrum both the sequence of the spin and parity values and the corresponding energies are reasonably well reproduced by the calculations.

As can be seen from Fig. 1, in addition to the good reproduction of the positive-parity states, the shell model is able to reproduce the energies of the lowest $1/2^-$ and $3/2^-$ states at 4055 keV and 5156 keV reasonably well, with calculated values of the energies at 3764 keV and 5137 keV, respectively. Not seen in the figure, the energy of the first $5/2^-$ state at 5438 keV is also well reproduced by the shell model, placing it at 5.433 keV. This is strong evidence that the size of the p-sd shell gap is correct in the adopted Hamiltonian.

The shell-model occupancies for the single-particle states in the active orbitals are given in Table II. The $0s$ shell is taken to be fully occupied. In Table III we show the results of the present calculations for the nuclear form factors $F_Z(q^2)$ and $F_N(q^2)$, calculated using the shell-model occupancies of Table II. The form factors are given by

$$F_Z(q^2) = \frac{1}{Z} \sum_j \sqrt{(2j+1)} \langle j || j_0(qr) || j \rangle \left(V_j^p\right)^2$$

$$F_N(q^2) = \frac{1}{N} \sum_j \sqrt{(2j+1)} \langle j || j_0(qr) || j \rangle \left(V_j^n\right)^2, \quad (7)$$

where p and n denote proton and neutron states, while the coherent form factors $S_N = N F_N$ and $S_Z = Z F_Z$, where $N = 14$ and $Z = 13$ are the neutron and proton numbers in the case of ^{27}Al. With respect to the previous shell-model results (see Ref. [12]), the present value of the coherent matrix element squared is smaller but still some 10% larger than the experimental value.

In Table IV we are listing the calculated values for the matrix elements of Eq. (3), for each of the processes, which may contribute to the muon-to-electron conversion. From the results given in the table it is seen that the calculated values are practically exhausted by the ground-state contributions to each process, and that the spin-independent vector channel is the dominant transition for all the processes considered. The analysis of the contributions to these matrix elements shows that they are given in almost equal parts by proton and neutron configurations, and that the main contribution, which yields a value practically equal to the final one is given by the ground state of the target nucleus.

TABLE IV. Vector (S_V) and axial (S_A) matrix elements. In the table we show the ground-state (g.s.) and total contributions to each quantity as well as the relevant matrix element M^2.

Process	S_V(g.s.)	S_V(total)	S_A(g.s)	S_A(total)	$M^2 = S_V + 3S_A$
W-exchange	664.9	665.1	0.0	0.371	666.20
SUSY Z-exchange	743.5	743.9	0.0	6.765	764.20
photonic	69.66	69.68	0.0	0.0	69.68

V. CONCLUSIONS

The measurement of muon-to-electron conversion process in nuclei is a convenient tool to establish limits on the lepton-flavor violation. The nucleus ^{27}Al is one of the nuclei of choice for performing the experiments, and due to it we have calculated the nuclear matrix elements for the operators entering the muon-to-electron conversion mediated by *W* exchange, SUSY particles, *Z* exchange, and photon exchange between nucleus and leptons with production of neutrinos. From our results, based on large-scale shell-model calculations of the wave functions of the participant nuclear states in Al, we confirm the dominance of spin-independent, coherent ground-state transitions, with practically no contributions from the excited positive-parity or negative-parity states.

ACKNOWLEDGMENTS

[1] W. J. Marciano and A. I. Sanda, Phys. Rev. Lett. **38**, 1512 (1977).

[2] W. Marciano and A. Sanda, Phys. Lett. B **67**, 303 (1977).

[3] J. Vergados, Phys. Rep. **133**, 1 (1986).

[4] V. Cirigliano, S. Davidson, and Y. Kuno, Phys. Lett. B **771**, 242 (2017).

[5] W. Bertl, R. Engfer, E. Hermes, G. Kurz, T. Kozlowski, J. Kuth, G. Otter, F. Rosenbaum, N. Ryskulov, A. van der Schaaf *et al.*, Eur. Phys. J. C **47**, 337 (2006).

[6] P. Wintz, *Proceedings of the First International Symposium on Lepton and Baryon Number Violation*, edited by H. V. Klapdor-Kleingrothaus and I. V. Krivosheina (Institute of Physics Publishing, Bristol, 1998).

[7] W. Honeckerw, C. Dohmen, H. Haan, D. Junker, G. Otter, M. Starlinger, P. Wintz, J. Hofmann, W. Bertl, J. Egger *et al.* (SINDRUM II Collaboration), Phys. Rev. Lett. **76**, 200 (1996).

[8] Yoshitaka Kuno (COMET Collaboration), Prog. Theor. Exp. Phys. **2013**, 022C01 (2013).

[9] D. Glenzinski (Mu2e Collaboration), AIP Conf. Proc. **1222**, 383 (2010).

[10] A. M. Baldini, Y. Bao, E. Baracchini, C. Bemporad, F. Berg, M. Biasotti, G. Boca, M. Cascella, P. W. Cattaneo, G. Cavoto *et al.*, Eur. Phys. J. C **76**, 434 (2016).

[11] B. Aubert, Y. Karyotakis, J. P. Lees, V. Poireau, E. Prencipe, X. Prudent, V. Tisserand, J. Garra Tico, E. Grauges, M. Martinelli *et al.* (BABAR Collaboration), Phys. Rev. Lett. **104**, 021802 (2010).

[12] T. Siiskonen, J. Suhonen, and T. S. Kosmas, Phys. Rev. C **62**, 035502 (2000).

[13] C. Dohmen, K.-D. Groth, B. Heer, W. Honecker, G. Otter, B. Steinrücken, P. Wintz, V. Djordjadze, J. Hofmann, T. Kozlowski *et al.*, Phys. Lett. B **317**, 631 (1993).

[14] T. Kosmas and J. Vergados, Nucl. Phys. A **510**, 641 (1990).

[15] T. Kosmas, G. Leontaris, and J. Vergados, Prog. Part. Nucl. Phys. **33**, 397 (1994).

[16] T. Kosmas, J. Vergados, O. Civitarese, and A. Faessler, Nucl. Phys. A **570**, 637 (1994).

[17] T. Kosmas and J. Vergados, Phys. Rep. **264**, 251 (1996).

[18] B. Wildenthal, Prog. Part. Nucl. Phys. **11**, 5 (1984).

[19] T. Siiskonen, J. Suhonen, and T. S. Kosmas, Phys. Rev. C **60**, 062501 (1999).

[20] T. S. Kosmas, A. Faessler, F. Šimkovic, and J. D. Vergados, Phys. Rev. C **56**, 526 (1997).

[21] T. S. Kosmas, A. Faessler, and J. D. Vergados, J. Phys. G: Nucl. Part. Phys. **23**, 693 (1997).

[22] A. Faessler, T. Kosmas, S. Kovalenko, and J. Vergados, Nucl. Phys. B **587**, 25 (2000).

[23] S. M. Bilenky and S. T. Petcov, Rev. Mod. Phys. **59**, 671 (1987).

[24] A. Bohr and B. R. Mottelson, *Nuclear Structure, Vol. I* (Benjamin, New York, 1969).

[25] R. Meharchand, R. G. T. Zegers, B. A. Brown, S. M. Austin, T. Baugher, D. Bazin, J. Deaven, A. Gade, G. F. Grinyer, C. J. Guess *et al.*, Phys. Rev. Lett. **108**, 122501 (2012).

[26] Y. Utsuno and S. Chiba, Phys. Rev. C **83**, 021301 (2011).

[27] E. K. Warburton and B. A. Brown, Phys. Rev. C **46**, 923 (1992).

[28] B. Brown and W. Rae, Nucl. Data Sheets **120**, 115 (2014).

[29] National Nuclear Data Center, Brookhaven National Laboratory, 2017, http://www.nndc.bnl.gov